Nonreactive spreading at high temperature: Molten metals and oxides on molybdenum

E. Saiz and A. P. Tomsia
Materials Sciences Division, Lawrence Berkeley National Laboratory, Berkeley, California 94720, USA

N. Rauch,* C. Scheu,† and M. Ruehle
Max Planck Institute für Metallforschung, Stuttgart, Germany

M. Benhassine, D. Seveno, and J. de Coninck
Centre for Research in Molecular Modeling, University of Mons-Hainaut, Mons, Belgium

S. Lopez-Esteban
Departamento de Materiales Particulados, Instituto de Ciencia de Materiales de Madrid, CSIC, Spain
(Received 21 June 2007; published 16 October 2007)

The spontaneous spreading of small liquid metal (Cu, Ag, Au) and oxide drops on Mo substrates has been studied using a drop transfer setup combined with high-speed video. Under the experimental conditions used in this work, spreading occurs in the absence of interfacial reactions or ridging. The analysis of the spreading data indicates that dissipation at the triple junction (that can be described in terms of a triple-line friction) is playing a dominant role in the movement of the liquid front. This is due, in part, to the much stronger atomic interactions in high-temperature systems when compared to organic liquids. As a result of this analysis, a comprehensive view of spreading emerges in which the strength of the atomic interactions (solid-liquid, liquid-liquid) determines the relative roles of viscous impedance and dissipation at the triple junction in spreading kinetics.

DOI: 10.1103/PhysRevE.76.041602 PACS number(s): 68.08.−p, 61.25.Mv

I. INTRODUCTION

Numerous modern technologies depend on the precise control of liquid spreading. In fields as diverse as the development of adhesives, soldering, coating fabrication, or oil recovery, the movement of a liquid front often controls the efficiency and stability of the process. Consequently, the scientific and engineering literature on the subject is extensive [1–7]. However, there seems to be a dichotomy between the research dealing with the room- or low-temperature spreading of organic liquids and polymers, and high-temperature systems such as molten metals or glasses. Like any other classification, this one is somewhat arbitrary—is the spreading of a solder or a polymer at 100–150 °C low or high temperature?—but it reflects a sense in the community that there are fundamental differences between high- and low-temperature liquids.

More surprising is that despite the fact that spreading at low or high temperature is, in principle, an equivalent phenomenon, very few papers have tried to bridge both areas of research. There are numerous experimental analyses of the spreading of molten metals and glasses, but, overall, the analysis of high-temperature spreading seems to lag behind its room-temperature counterpart. High-temperature data are very often difficult to interpret and sometimes contradictory [4,8–14]. This is in part due to the experimental difficulties associated with the manipulation of high-temperature liquids. While it is possible to study the spontaneous or forced spreading of organic liquids using a wide range of configurations (spontaneous droplet spreading, capillary rise, curtain coating, etc.) in a fast and economical way, studies with molten metals and ceramics need to be performed under carefully controlled conditions (in particular, temperature and atmosphere) and often demand complex experimental setups. The number of accessible experiments is much more limited. Up until now, sessile drop experiments are probably the most-used tests for the analysis of high-temperature spreading; however, this setup presents numerous complications that make the interpretation of the results difficult, starting with the fact that the drop melts on the same substrate on which wetting will be analyzed [15]. The theoretical analysis also has some added difficulties. Most analyses of liquid-solid wetting in low-temperature systems, including Young-Laplace equation, are based on the assumption that the substrate is an ideal solid, perfectly rigid and insoluble (nonreactive spreading); this is an excellent approximation for most low-temperature systems, but it does not describe many situations at high temperature in which spreading is often accompanied by interdiffusion and chemical reactions [16–24].

TABLE I. Glass compositions (in wt %). Glass *G*Ti has an addition of 3 mol % TiO_2 compared to the composition of glass *G*.

	SiO_2	CaO	Al_2O_3	TiO_2
G	62.00	23.00	15.00	0.00
*G*Ti	59.63	22.15	14.42	3.80

*Present address: Department of New Materials and Biosystems, Max Planck Institute für Metallforschung, Stuttgart, Germany.

†Present address: Department of Physical Metallurgy and Materials Testing, Montanuniversität Leoben, Leoben, Austria.

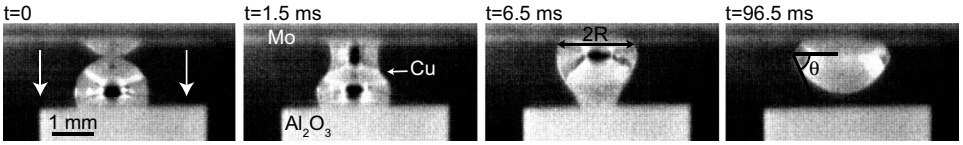

FIG. 1. Sequence of pictures taken during a drop-transfer experiment showing the spreading of a small Cu drop on Mo at 1100 °C (the camera speed was 4000 fps).

The goal of this work is to establish the basis for a systematic analysis of the spreading of molten metals and glasses that will help to bridge the high- and low-temperature fields. This paper focuses on the study of the spontaneous spreading of metal and glass droplets on Mo substrates. The selected systems exhibit a nonreactive behavior, and comparisons between systems with standard theories are straightforward. Even though low- and high-temperature liquids share some characteristics, they also have important fundamental differences: While the viscosities can be similar, molten metals and oxides have typically 1–2 orders of magnitude larger surface tensions and works of adhesion, due to much stronger atomic interactions. The comparison of high- and low-temperature data will help to determine the relative weight of the different physicochemical factors (viscosity, solid-liquid interactions, surface tensions, etc.) that affect the movement of the liquid. In particular, it will allow a systematic discussion of the roles of the viscosity (the main parameter in continuous hydrodynamic theories) [25] and the atomic dynamics close to the solid-liquid-vapor triple junction (typically described using molecular-kinetics theories) [26]. This approach can provide critical information for the development of a unified model where all the contributions can be incorporated. It could also serve as the first step in the formulation of a predictive theory to describe the spreading of the reactive liquids that play a critical role in many advanced technologies such as brazing or the fabrication of composites.

II. EXPERIMENT

The nonreactive spreading of liquid fcc metals (Ag, Au, Cu)[1] and silicate glasses on polycrystalline[2] and single-crystalline[3] molybdenum substrates was analyzed using a drop-transfer setup inside a side-loading furnace (series 15, CENTORR Vacuum Industries, Nashua, NH, USA) with a tungsten heating element. The experiments were performed under controlled oxygen activity by flowing Ar/H_2 mixtures at $\sim 2\times 10^{-5}$ m^3 s^{-1} [$p(Ar)\approx 10^5$ Pa]. The oxygen content of the gas leaving the furnace was monitored using a ZrO_2 sensor (Centorr, model 2D, USA). In all the experiments with liquid metals, the oxygen content in the gas was kept below 1×10^{-14} ppm [$p(O_2)<10^{-20}$ atm]. The experiments with SiO_2-CaO-Al_2O_3-TiO_2 glasses (the compositions are listed in Table I) were carried out at 1200 °C in oxygen partial pressures ranging between 10^{-16} and 10^{-19} atm in order to avoid Mo oxidation and reactions between the substrate and the glass. The glasses were prepared following a conventional procedure described in detail elsewhere [27]. At this temperature, the oxides are molten and behave similar to a highly viscous liquid; their spreading was also studied using the sessile drop configuration.

Prior to the tests, the polycrystalline molybdenum substrates ($\sim 10\times 12$ mm, 1 mm thick) were annealed at 1350 °C for 15 min in order to recrystallize the Mo and subsequently ground with 450 μm SiC to remove the grain boundary groves that formed during the heat treatment. All the substrates, polycrystal and single crystal ($\sim$1 cm diameter), were either mechanically or electrolitically polished. For the mechanical polishing, the Mo surfaces were ground with 1200 μm SiC paper, and afterwards polished on an automatic polishing machine down to 1 μm diamond. Electrolitical polishing was performed in a LektroPol-5 machine (Struers, Germany). The electrolyte was a mixture of 875 mL of methanol (99.8 %) and 125 mL H_2SO_4 (95–97 %). The H_2SO_4 was carefully added to the methanol in a stepwise fashion in order to avoid strong exothermic reactions. The polished area was a circle of 0.9 cm diameter. The samples were polished for 90 s at 20–22 °C, using a voltage of 18 V. Six hundred milliliters of fresh electrolytes were used for each polishing cycle. Before the experiments, the metals, glasses, and Mo substrates were cleaned with acetone and ethanol in an ultrasonic bath, and dried with an air gun.

Drop transfer tests were performed using the following procedure. A small piece ($\sim$0.1–0.2 g) of liquid metal or glass was placed on a nonreactive substrate (sapphire for liquid metals, and boron nitride for the glasses) where the liquids exhibit an obtuse contact angle inside the furnace (Fig. 1), and the Mo substrate was placed on a molybdenum holder situated $\sim$10–15 mm above it. Subsequently, the furnace was evacuated to a pressure of $\sim 6\times 10^{-4}$ Pa, and refilled with gas. Before heating, the gas was flown for $\sim$2 hours while its oxygen content was monitored in order to assure that the required $p(O_2)$ was reached. The assembly was heated at 15–25 °C min^{-1} to the test temperature. At that temperature, the surface of the liquid metals was shiny, indicating that it was not covered by an oxide layer. Two types of experiments were carried out: "equilibrated" and "nonequilibrated." For equilibrated tests, the Mo substrate was lowered and placed in close proximity to the liquid surface ($\sim$1 mm or less) for 1 h. Afterwards, the substrate was lowered slowly until it just touched the drop surface and the liquid spread on it, transferring from the ceramic plate to the molybdenum (Fig. 1). In case of the nonequilibrated experiments, as soon as the required temperature was reached, the

[1]Ag, 99.9%, Johnson Mattey, USA; Cu, 99.8%, Aldrich, USA; Au, 99.99%, Johnson Mattey, USA.

[2]99.9% Aldrich, USA.

[3]Accumet Materilas, USA.

TABLE II. Comparison of the composition (in wt %) of the single and polycrystalline Mo substrates determined with ICP-OES

	Cr	Ca	Fe	Cu	Mg	Ni	Zn	Zr
Single crystal	<0.001	~0.006	~0.005	~0.015	<0.0001	~0.005	~0.002	~0.007
Poly crystal	<0.001	<0.002	<0.001	<0.001	<0.0001	<0.001	<0.0005	<0.001

Mo was put in contact with the liquid, and the spreading experiment was performed. Spreading was recorded through a transparent quartz window using a high-speed motion analysis system (Photron 512 PCI fastcam) with a digital camera able to take up to 32 000 frames per second, and an optical system with a magnification ranging between ×5 to ×20 (corresponding to pixel sizes between ~40 to 10 μm). The contact angles and drop radius were measured using a program developed in our laboratory to fit the drop profile [28]. For the sessile-drop experiments with glasses, a small piece of glass was placed on the Mo substrate inside the furnace, and the assembly was heated to 1200 °C at 25 °C min^{-1}.

Before and after the experiments, the Mo surfaces were analyzed using scanning electron microscopy (Hitachi, S-4300SE/N, Japan) with associated chemical analyses (Noran System Six, Thermo, USA) by energy dispersive spectroscopy (SEM-EDS), atomic force microscopy (AFM) in the constant-force mode (Hysitron Corp, USA), scanning probe microscopy (TopoMetrix, TMX 2000, USA), and Auger electron spectroscopy (AES, JEOL JAMP-7830 F). Compositions of the Mo substrates were determined by inductively coupled plasma-atomic emission spectrometry (ICP-AES), and the grain orientation by orientation imaging microscopy (OIM). After the experiments, the surface of the drops and cross sections polished with 0.3 μm Al_2O_3 were analyzed using optical microscopy and SEM-EDS. Transmission electron microscopy (TEM) of the cross sections was performed in a JEOL 2000 FX microscope. TEM samples were prepared by focused ion beam (FIB, Work station 200, FEI). The surface of the sample was sputtered with a chromium layer in order to protect the triple line of the sample; thus, the sample was protected against shadow effects in the FIB, and diffusion of the gallium ions from the ion beam. Due to the chromium coating, it was not necessary to coat the sample with tungsten or platinum as it is usually done for FIB investigations. For the cross section, an area of 173 μm^2 was cut with an acceleration voltage of 30 kV and an ion beam current of 2.7 nA. The cut was done with an acceleration voltage of 6 kV, and an ion beam current of 12 pA. A TEM lamella was cut out of the sample using the FIB, and placed on a copper grid for observation using microtweezers.

III. RESULTS AND DISCUSSION

A. Microstructural observations

The composition of the Mo substrates used in this study is summarized in Table II. Overall, the single-crystal substrates seem to contain a slightly larger amount of impurities. Auger analyses of the surface of the polished substrates showed only the presence of Mo, C, and O. In order to obtain more detailed information about the polycrystalline Mo surface, such as grain size and orientation, OIM measurements were performed. The average grain size is between 21–43 μm. About 50 % of all the grains have a (311) orientation, with an error of 15°. Around 20–25 % of the grains have orientations (111) and (100). Less than 3% of the grains have a (110) orientation. The substrates have a roughness (average peak to valley distance) of 70–100 nm independently of the polishing procedure; however, the surfaces obtained using electrolitical polishing are much smoother (Fig. 2).

Cross-sectional analysis of the drop and/or substrate interface after spreading did not show any sign of interdiffusion (Fig. 3). All the selected systems are simple eutectics in which there is a negligible solubility of the metals in Mo, and the solubility of Mo in the liquids is <3 wt % at the experimental temperatures. Furthermore, the experimental temperatures are at least 1300 °C below the melting point of Mo. For glasses, the equilibrium oxygen partial pressure for the reaction

$$3Mo + SiO_2 \rightarrow Mo_3Si + O_2(g)\uparrow \quad (1)$$

is $\sim 10^{-19}$ atm at 1200 °C and even lower for the other glass components [29]. For the $p(O_2)$'s used in these experiments, no chemical reactions or measurable interdiffusion between the glass and the metal was observed.

After the spreading of liquid metals, a ring of small metallic drops was observed surrounding the edge of the solidified liquid front at a distance of 2–10 μm (Fig. 4). The drops are typically <2 μm in diameter. It seems that the liquid metal front overshoots during spreading and recedes again, leaving a ring of small droplets. This can happen due to a breakup of the droplet during transfer. Auger analyses of the substrate ahead of the liquid front showed the presence of liquid atoms or molecules adsorbed on the free Mo surface

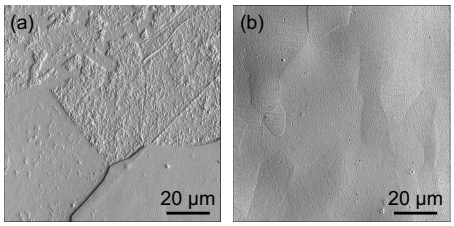

FIG. 2. AFM images of (a) mechanically and (b) electrolitically polished Mo.

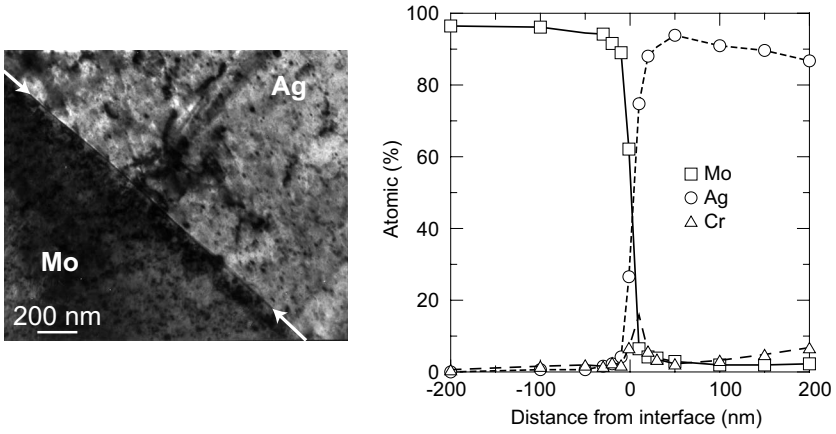

FIG. 3. Transmission electron micrograph and associated EDS analysis across the Ag-Mo interface. The interface is sharp (see white arrows) and there is no evidence of Mo-Ag interdiffusion.

after the spreading tests. None of the characterization techniques showed evidence of the formation of triple-line ridges that could affect the spreading kinetics [30,31].

B. Equilibrium contact angle

The dependence of the final contact angle on temperature was much stronger than what is typically expected from the known variation of the metal surface energies (Fig. 5) [32]. A sharp increase in contact angle was observed for molten Cu and Ag at temperatures below ~1100 °C during nonequilibrated experiments. At the temperature 1100 °C, there was a large difference between the final angles reached in the equilibrated and nonequilibrated cases. The oxygen partial pressures during the experiment were much lower than the ones required for the oxidation of molybdenum (between 10^{-16} and 10^{-10} atm at 950 °C and 1300 °C, respectively) [29]. However, the results are consistent with the presence of a layer of excess impurities (oxygen and carbon, according to the Auger analysis) on the Mo surface that can only be eliminated after firing in Ar/5% H_2 at temperatures above ~1000 °C. These results are in agreement with previous reports that show a strong dependence of the final contact angle of low-melting-point metals on Mo and W with the atmosphere [4,33–35]. According to Allen, temperatures above 1000 °C are required to eliminate oxygen from the Mo surface at a total pressure of 10^{-3} Pa [36]. The comparison between the final contact angles reached by silver in equilibrated and nonequilibrated experiments shows that eliminating impurities from the polycrystalline Mo surface takes several minutes at 1070 °C in Ar/5%H_2. It could also be observed that cleaner surfaces can be achieved on single-crystal substrates, at lower temperatures.

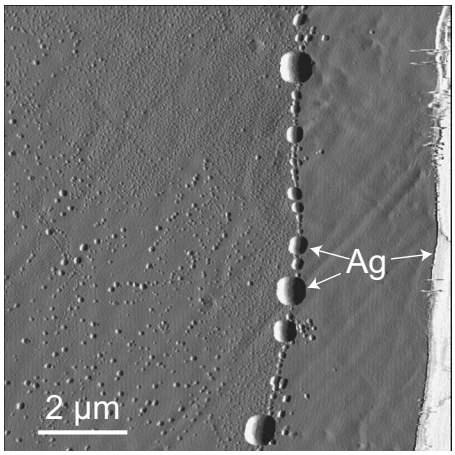

FIG. 4. AFM image of the edge of a silver drop on Mo after an experiment performed at 1070 °C. A ring of microscopic drops surrounds the "frozen" liquid front (in the right of the image). The fast solidification of the liquid metal during cooling allows the observation of these frozen microscopic droplets in the atomic force or scanning electron microscopes something that cannot be easily done after experiments with organic liquids.

The spreading times used in these experiments are too short to allow interdiffusion at the solid-liquid interface. Under these conditions, and assuming that under our experimental conditions some degree of adsorption can occur, the measured contact angle will be somewhere between the values related to the thermodynamic work of adhesion (W_{ad}) between equilibrated phases, and the work of separation (W_{sep}) between pure materials [37]. Experiments performed for much longer times in these systems resulted in similar values of the final contact angle [38], and it has been suggested that in systems with small mutual solubility, the works of adhesion and separation are relatively close [18,38]. In the following discussion, we will use the final contact angles measured in our experiments to estimate the work of adhesion, but the difference in conditions should be kept in mind.

Single-crystal wetting experiments showed that wetting is better on (110) surfaces than on the (100) plane (Fig. 5). According to several calculations [39,40], the surface energy of the (100) plane of Mo (γ_{sv}^{100}=3.34–3.52 J m^{-2}) is larger than the one of the (110) plane (γ_{sv}^{110}=2.92–3.14 J m^{-2}). Then

$$\cos\theta_0^{110} > \cos\theta_0^{100} \Rightarrow \gamma_{sl}^{100} - \gamma_{sl}^{110} > \gamma_{sv}^{100} - \gamma_{sv}^{110} > 0, \quad (2)$$

where γ_{sl} is the corresponding solid-liquid interfacial tension and θ_0 the equilibrium contact angle. The solid-liquid inter-

TABLE III. Final contact angles on "clean" polycrystalline Mo surfaces. The heat of evaporation of molybdenum is 590.3 kJ mol^{-1}.

Liquid	Temperature T (°C)	Cont. Angle θ_0 (deg)	Surf. En. γ_{lv} (J m^{-2})[32]	Viscosity η (Pa s)[32]	Density ρ (Kg m^{-3})[32]	Ω_{Me-Mo} (kJ mol^{-1})[91]	L_s (kJ mol^{-1})[78]
Ag	1070	26±3	0.9	3.3×10^{-3}	9250	148	251.2
Ag	1150	13±3	0.885	3.0×10^{-3}	9175		
Ag	1290	11±3	0.856	2.5×10^{-3}	9050		
Au	1100	24±3	1.138	5.0×10^{-3}	17300	13.5	342.4
Cu	1150	23±3	1.36	4.0×10^{-3}	7950	74.5	340.8
Sn [51]	1190	~10	0.467	$\sim1\times10^{-3}$	6400	83.5	296.4
G	1250	39±3	0.482	350	$\sim10^3$		
*G*Ti	1250	30±3	0.39	350	$\sim10^3$		

facial energies follow the same ranking as the surface energies, but the differences are more accentuated. Using a quasichemical approach of the type pioneered by Skapski [41], it is possible to estimate the surface energy of the solid as

$$\gamma_{sv} = -\frac{z - z_s}{2\omega}\varepsilon_{ss}, \tag{3}$$

where z is the coordination number of the crystal ($z=14$ for a bcc crystal such as Mo); z_s is the number of bonds of an atom in the plane; and ω is the area per atom in the surface. The factor 2 in the denominator comes from the fact that two surfaces are created by dividing the crystal, and ε_{ss} is the bond energy of the solid that can be approximated by $-2L_s/zN$ (L_s being the heat of sublimation and N the Avogadro number). In the (100) surface, there are four nearest-neighbor broken bonds and one next-nearest-neighbor broken bond; in the (110) plane, there are two of each of the broken bonds. By this simple model, it can be understood why the (100) plane should have a larger surface energy, since it has more broken bonds, assuming that ω is similar for both planes. Using the same quasichemical approach, the work of adhesion, W_{ad}, can be written as

$$W_{ad} = -\frac{(z - z_s)}{\omega}\varepsilon_{sl}, \tag{4}$$

where ε_{sl} is the bond energy of the solid-liquid atoms. According to Eq. (4), $W_{ad}^{100} > W_{ad}^{110}$, opposite of the experimental observation $\frac{W_{ad}^{110}}{W_{ad}^{100}} \approx 1.05-1.10$. It also seems to contradict the trend observed in the wetting of some liquid metals on their own solids [42], where the high-index planes exhibit lower contact angles. This result points out to the limitations of the quasichemical approach that, among other things, ignores mutual adsorption and entropic effects. Adsorption and segregation usually play an important role in high-temperature wetting [9,43–50]. Auger analysis of the free surface of Mo after the experiments indicates that adsorption of liquid atoms or molecules is probably decreasing the energy of the solid-vapor interface.

Table III summarizes the final contact angles measured for each system under the conditions that give the cleaner molybdenum surface, and the corresponding work of adhesions are shown in Fig. 6 [51]. For comparison, the graph also plots the measured work of adhesion for the stoichiometric interfaces between those metals and an aluminium

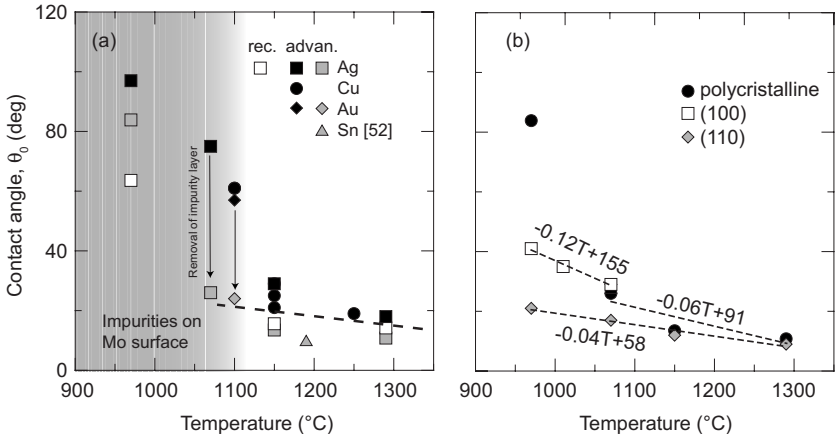

FIG. 5. (a) Dependence of the contact angle of molten metals on Mo with temperature. The black symbols corresponds to experiments performed under "nonequilibrated" conditions. The grey symbols correspond to "equilibrated" experiments. Open symbols correspond to receding contact angles from Ref. [39]. (b) Dependence of the contact angle of silver on Mo with crystal orientation. According to the fittings the contact angle will became zero for temperatures between 1300–1500 °C

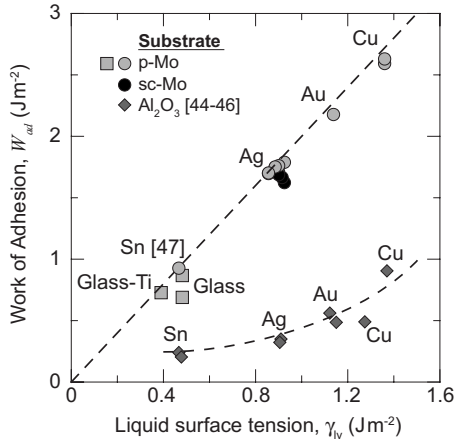

FIG. 6. Calculated work of adhesion for the different liquids on polycrystal (p-Mo) and single crystal (sc-Mo) molybdenum. Each data point corresponds to a single experiment. The dashed line represents $W_{ad}=2\gamma_{lv}$. Data for the same metals on Al_2O_3 (diamonds) are also presented for comparison.

oxide [48–50,52]. As expected, the works of adhesion in the metal metal systems are larger than those from the oxide metal. It is well known that in nonreactive cases, liquid metals show obtuse contact angles on ceramics [31,48]. On the other hand, molten oxides tend to exhibit low contact angles on the metals [4,27,53,54], a fact that is usually attributed to their low surface tension [4]. The contact angles are slightly lower for glasses with TiO_2 (Table III). Since the addition of 3 mol % TiO_2 had a negligible effect on the surface energy of the molten glass [27], the observed decrease of the equilibrium contact angle for glasses with TiO_2 additions can only be explained by the preferential adsorption of TiO_x species at the solid liquid interface. Titania additions decrease the contact angle of silicate glasses on Pt in air [55] and there is ample evidence of adsorption of Ti species at the interface between liquid metals and solid oxides. This effect has been attributed to their polar nature [9,28,34,56]. Typically, oxygen is adsorbed on a metal surface at oxygen partial pressures that are 3 to 8 orders of magnitude below the critical one for bulk metal oxidation [48]. The oxygen partial pressures used in the glass experiments are only 1 to 2 orders of magnitude below the ones required for the oxidation of Mo. Oxygen adsorption could be expected on the Mo surface equilibrated with that atmosphere. In experiments with liquid metals, the $p(O_2)$ in the furnace is at least 6 to 10 orders of magnitude lower than the one required for oxidation, and it is likely that the molybdenum surface is free of adsorbed oxygen.

C. Spreading kinetics

1. Spreading of metal drops

Spreading of the metallic drops took ~10–20 milliseconds. No significant differences were observed between the spreading kinetics on substrates polished mechanically or electrolitically. Typical data recorded during spreading can be observed in Fig. 7. Initially (around the first 8 to 12 ms) the drop spreads continuously, forming a bridge between the alumina and the molybdenum substrate. Later, a thin liquid neck develops between the two substrates. This neck breaks causing a sudden stop of the liquid front accompanied by oscillations of the drop and the contact angle. In all systems, the data taken during the continuous spreading is very reproducible, independent of the drop size (typically between 1 to 3 mm in diameter) and will be analyzed in detail.

During the deposition of a small nonreactive liquid drop on a flat substrate, three regimes can be distinguished (Fig. 8): impact, inertial, and capillary. During the impact regime, the drop hits the substrate, and flow is driven by the dynamic pressure of impact and resisted by inertia. In the inertial regime, flow is driven by the capillary force imbalance at the triple line, but the capillary-induced spreading is much faster than the impact velocity, the drop does not exhibit a constant curvature shape, and the surface curvature could add an extra driving force, while inertia contributes to resist spreading. Finally, during the capillary regime, the drop has a constant curvature shape, and the driving force for spreading is the difference between the instantaneous dynamic contact angle

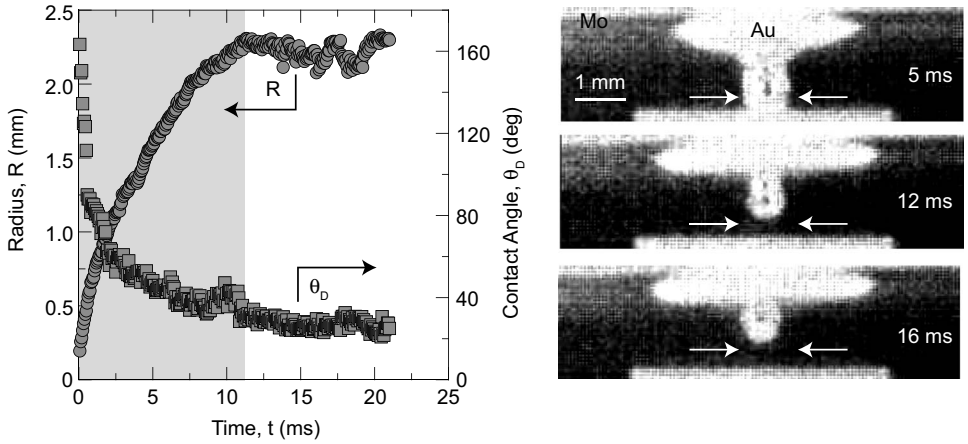

FIG. 7. Variation of the contact angle and the radius of a Cu drop on Mo during drop transfer at 1150 °C. The grey area corresponds to the continuous spreading before the break up of the liquid bridge between the top and bottom substrates (compare the region indicated with the white arrows in the pictures shown on the right corresponding to a gold drop spreading at 1100 °C).

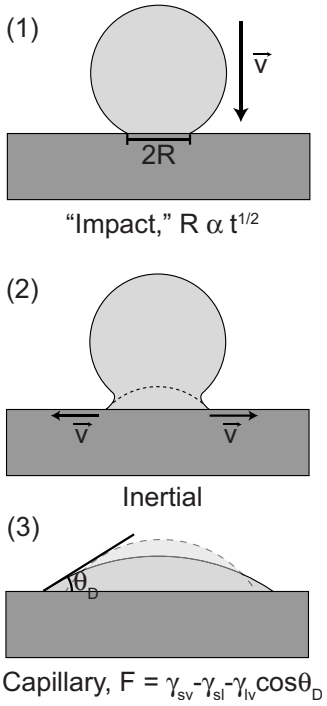

FIG. 8. Regimes of the spontaneous continuous spreading of a liquid drop on an ideally rigid and insoluble substrate.

and the equilibrium one [57–61]. The relative duration of the regimes depends on several factors such as the kinetic energy of the drop, viscosity, and surface tension.

During continuous spreading, the contact radius of the small metallic drops was proportional to $t^{1/2}$ (Fig. 9). It has been observed that for the impact regime [57,58]

$$R \approx (R_{drop} V t)^{1/2}, \tag{5}$$

where R_{drop} is the radius of the initial spherical drop and V the approaching velocity of the drop on the surface. In our experiments, R_{drop} is of the order of 10^{-3} m, and V $\sim 10^{-4}$ m s^{-1} (or even lower). The expected value of $R_{drop}V$ ($\sim 10^{-7}$ m^2 s^{-1}) is much smaller than what we measure experimentally ($\sim 10^{-4}$ m^2 s), and it can be concluded that the drop is not spreading in the impact regime as expected from the very slow approaching velocities.

The Weber number ($We = \rho V^2 R_{drop}/\gamma_{lv}$, where ρ is the density of the liquid) is a measurement of the driving force for spreading, in particular, the relative importance of the impact driving force (dominant for large We) and the capillary forces (controlling at low We). Inertial effects are more important for systems with decreasing Ohnesorge number [$Oh = \eta/(\rho R_{drop}\gamma_{lv})^{1/2}$ where η is the liquid viscosity] [61,62]. The physical conditions of the drop transfer experiments with small metallic drops result in Webber and Ohnesorge numbers that are much lower than 1 (Table III). The drop spreads in the inertial regime, and droplet breakup and oscillations can be expected [61,62]. The oscillations arise from the pressure gradients that form in a system where capillary-driven spreading is much faster than the approaching velocity of the drop, and where, due to the low viscosity, the oscillations damp out on a time scale much longer than the spreading regime's. An exponential decay of the type proposed by Schiaffino and Sorin [61,62] can be used to fit the contact radius of the drop, R, in this regime,

$$R = 2.4 R_{drop}[1 - e^{-0.9t/\sqrt{\rho R_{drop}^3/\gamma_{lv}}}] + R_0. \tag{6}$$

An adequate fitting can be obtained using this expression, although some deviation from the data can be observed at times below 1 ms (Fig. 9). The physical parameters deduced from this expression are consistent with the experimental conditions: $R_{drop} \sim 0.5-1$ mm; R_0 (the initial contact radius used to compensate for the uncertainty in the contact time) $\sim 10-100$ μm, of the order of the pixel size in our experimental setup; and $\rho/\gamma_{lvn} \sim 10^4-10^5$ s^2 m^{-3} (of the order of the expected value, but in some cases, it could be different by an order of magnitude). Recent analyses of the transfer of waterdrops on glass substrates have reported R $\alpha\, t^{1/2}$ [58]. In their analysis of this phenomenon, Biance *et al.* [58] have

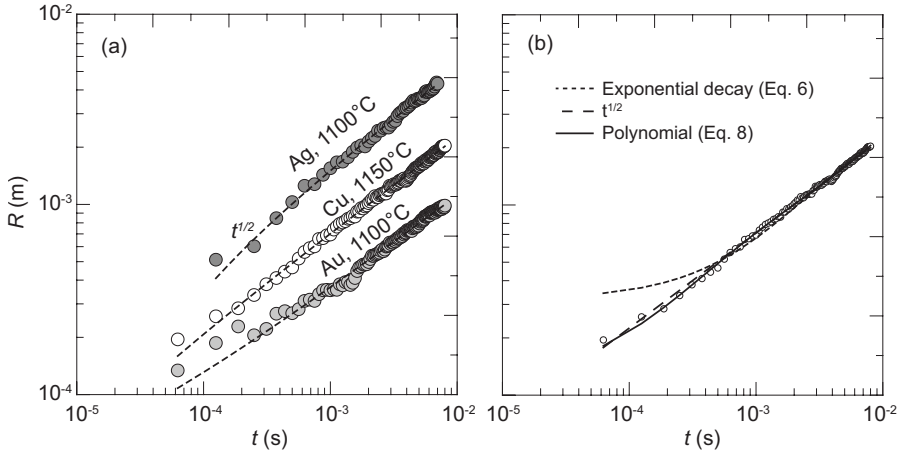

FIG. 9. (a) Variation of the drop radius with time for small metallic drops transferred to a Mo substrate. The dashed lines correspond to $t^{1/2}$ fittings. (b) Comparison of the different fittings for a Cu drop spreading on Mo at 1150 °C. The results are very similar, but the exponential decay seems to deviate at very short times (<1 ms). The polynomial fitting [Eq. (8)] provides reasonable values of the initial and final drop contact radius ($\sim 10^{-5}$ and $\sim 10^{-3}$ m, respectively).

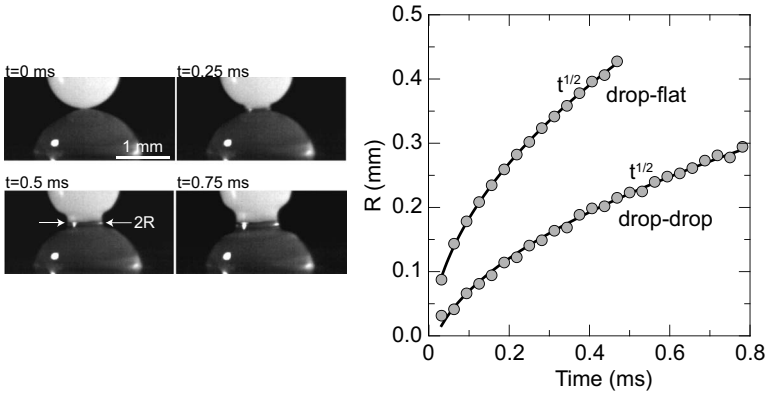

FIG. 10. Coalescence of two water drops (the drop on top has 5 wt % of nanosized alumina particles to help visualize the process). A neck forms between drops whose width evolves as $t^{1/2}$. The time dependence is the same for a drop impinging with a flat liquid surface or for the coalescence of two drops.

argued that spreading is occurring in an inertial regime. Due to the presence of a liquid film covering the glass, the phenomenon is equivalent to the coalescence of a liquid drop with a flat liquid surface [63–65]. In this situation, a small neck forms between the liquid surfaces (Fig. 10) and has a radius that grows according to

$$R = \left(\frac{\gamma_{lv} R_{drop}}{\rho}\right)^{1/4} t^{1/2}. \tag{7}$$

Since, for liquid metals, $\gamma_{lv} \sim 1$ J m^{-2} and $\rho \sim 10^4$ Kg m^{-3}, Eq. (7) will result in $R \sim 10^{-7/4} t^{1/2}$, which is close to the values observed experimentally. In addition, the images confirm that the small metallic drop does not show a constant curvature shape during transferring; however, in the metal cases, there is no evidence of the presence of a liquid metallic film covering the substrate prior to the transfer even after equilibrated experiments in which the substrate has been kept in close proximity to the top of the liquid drop for up to 1.5 hours. These data would suggest that despite the physical differences (a drop spreading on a solid vs a drop spreading on a liquid or two liquid drops coalescing) the drop is spreading in an inertial regime, and that the dependence of the contact radius of the drop with time can be described by using the same law for the liquid-liquid and solid-liquid case; however, there are differences: The initial stages of coalescence between two liquid surfaces are characterized by the formation of a thin liquid neck whose diameter grows with time, and the driving force is proportional to the liquid surface tension. During the spreading of a droplet on a solid, the liquid front forms a finite dynamic contact angle, θ_D, with the substrate. The dynamic contact angle decreases continuously over time, towards an equilibrium value (Fig. 7) with the consequent decrease in the spreading driving force.

These previous analyses did not contemplate the physical phenomena that govern the conditions at the dynamic triple junction. For example, in a continuous approach, they do not specify the mechanisms that relieve the nonslip condition in an area close to the triple junction and the corresponding stress singularity. Assuming that, at least in a first approximation, the relationship between the dynamic contact angle (θ_D) measured in an area of 100–200 μm around the triple junction, and the speed of the liquid front (v) is independent of the macroscopic flow conditions, we can use spreading models developed for forced and spontaneous spreading to investigate physical processes that control the movement of the triple junction. While there is still some discussion regarding the role of the far-field fluid flow conditions, we will discuss below how the corrections to the models used in this analysis could be relatively minor.

Analysis of spreading is typically done by compensating the driving force for spreading with the controlling channels of dissipation. Usually three channels are considered, either dissipation in the close vicinity of the solid near the wetting line, the viscous impedance in the bulk of the drop, or the viscous dissipation in a precursor film associated with the complete wetting case ($\theta_0 = 0$). By identifying the dominating dissipation mechanisms, it is possible to write the local relationships between the dynamic contact angle and the speed of the liquid front [1,25,26,66–70].

In order to apply these relations to the analysis of drop transfer, the speed of the liquid front was estimated by using an empirical fitting for the contact radius of the drop,

$$R = \frac{p_0 + p_1 t + p_2 t^2}{1 + p_3 t + p_4 t^2}. \tag{8}$$

This fitting reproduces well the observed evolution of the contact radius for the complete time range of the measurements. Opposite to a $t^{1/2}$ fitting, this equation provides parameters with some physical meaning as the time approaches 0 or infinity. As $t \to \infty$, the drop radius reaches some finite value (p_2/p_4), and at the first point measured ($t=0$), the radius has already some finite value (p_0). It also provides a finite maximum velocity as $t \to 0$. To estimate the speed from the radius data, we used the so-called Bootstrap method [71]. With this powerful method, the original experimental data are used as the basis for a Monte Carlo simulation. From the original data set, randomly chosen points are replaced by duplicates. The duplicate points are chosen according to a normal distribution function, with the original data as the average, and the expected error on each datum point as the standard deviation. In this way, we replace the original set of data with a new one, for which the corresponding parameters

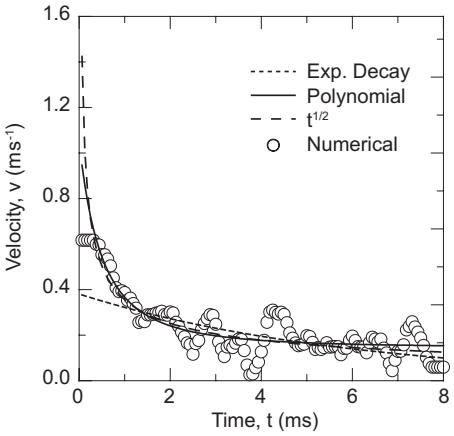

FIG. 11. Spreading velocities calculated using different fittings. The data corresponds to Cu spreading on Mo at 1150 °C [Fig. 9(b)]. The maximum velocities calculated from the polynomial fitting ($\sim 0.5-1$ m s^{-1}) are of the order of those recorded experimentally.

are then fitted with the method described above. Successive cycles result in a simulated set of values for each parameter. If enough cycles are used (>100), these sets turn out to be normally distributed, providing us with the mean value and standard deviation for the corresponding speed. The expected errors on each datum point were fixed at 3%. Figure 11 compares the results for the different radius fittings for a typical experiment. The "numerical" velocity values are calculated using a Savitzky-Golay smoothing method that performs a local polynomial regression of the second order around each point; in this case, four points have been taken around each data point [72]. It can be observed that, with the exception of a few initial points, the results are comparable. To further test the accuracy of this method, Benhassine *et al.* [73] have fitted theoretical radius and angle curves generated by using a fixed set of parameters; the difference between the starting parameters and the values obtained with the fitting is always lower than 8%.

The liquid metal drops exhibited a small but finite contact angle on Mo (partial wetting), and the experiments did not show any evidence of the formation of precursor films. The spreading velocities were much faster than the estimated critical velocity for the nucleation of a triple-line ridge on a Mo substrate, which agrees with the "postmortem" microstructural analysis [27]. This is a case of nonreactive spreading where the liquid front moves on a flat unreacted surface. In such a case, if the viscous impedance is the main channel of dissipation, the dynamic contact angle and speed of the liquid front, v, can be related using an equation of the type [25,66,67,74]:

$$g(\theta_D) = g(\theta_0) + 9\,\mathrm{Ca}\left[\ln\left(\frac{L}{L_s}\right) + Q\right], \tag{9}$$

where $\eta v/\gamma_{lv}$ is the capillary number (Ca). This analysis assumes that the liquid slips on the solid in a region of length L_s near the wetting line, with L being the distance from the triple line where the dynamic contact angle θ is measured, Q the dissipation in the slip region, and g a rather complex integrand. Still, it is assumed that Q is small, again minimizing the role of the dissipation in this zone. In Cox analysis [66] and in a first approximation, the macroscopic contact angle can be calculated without solving for a specific flow field and interfacial shape outside the cutoff region or specifying a cutoff mechanism in the inner region. While in most approaches θ_0 is taken as the equilibrium contact angle, Voinov already pointed out that it can also be a microscopic angle, θ_m, that can itself be velocity-dependent due to possible nonhydrodynamic mechanisms [67].

For small contact angles, Eq. (9) simplifies to

$$\theta_D^3 = \theta_0^3 + 9\,\mathrm{Ca}\left[\ln\left(\frac{L}{L_s}\right) + Q\right]. \tag{10}$$

These relationships have been deduced for the case in which inertia is negligible, and the liquid is in steady motion. These approximations could not describe very well the case of a millimeter metal drop spreading at velocities close to $0.1-1$ m s^{-1}. Using the drop radius as a characteristic length for the systems, the corresponding Reynolds number, Re, is 10^3-10^4. Cox has modified the analysis to account for inertial effects [75]. A key parameter in a Cox analysis is $\Gamma = \mathrm{Ca}/\mathrm{Re}$, which for the small liquid metal drops is $\sim 10^7$. However, in all cases, the experimental spreading speeds are much lower than those expected from hydrodynamic models (with or without inertial corrections) using reasonable values of L/L_s (Fig. 12).

These results suggest that dissipation processes occurring in the close vicinity of the contact line are playing a determining role. Blake [26,68,76] described this dissipation at the triple junction using a reaction-rate model in which the contact line motion is controlled by the displacements (of length λ) of the liquid molecules from one adsorption site to another on the solid surface. If spreading is driven by the capillary forces, $\gamma_{sv}-\gamma_{sl}-\gamma_{lv}\cos\theta_D$, this approach leads to the following relationship between the spreading kinetics and the dynamic contact angle:

$$v = 2K_0\lambda \sinh\left(\frac{\gamma_{lv}(\cos\theta_0 - \cos\theta_D)}{2nkT}\right), \tag{11}$$

where K_0 is an equilibrium frequency of the atoms in the triple junction; n is the number of adsorption sites per unit area; λ is the average distance between sites ($\lambda \sim n^{1/2}$); and k is the Boltzman constant. If ΔG_w is the molar activation free energy of wetting, then

$$K_0 = \left(\frac{kT}{h}\right) e^{-\Delta G_w/NkT}. \tag{12}$$

Additional driving forces that can act directly on the atoms at the triple line can be also included in Eq. (11). These forces can be written as a function of the speed of the liquid front, leaving the relationship between the dynamic contact angle and the spreading velocity as [26]

$$v = 2K_0\lambda \sinh\left(\frac{\gamma_{lv}(\cos\theta_0 - \cos\theta_D) + \varphi(v)}{2nkT}\right). \tag{13}$$

In addition, if

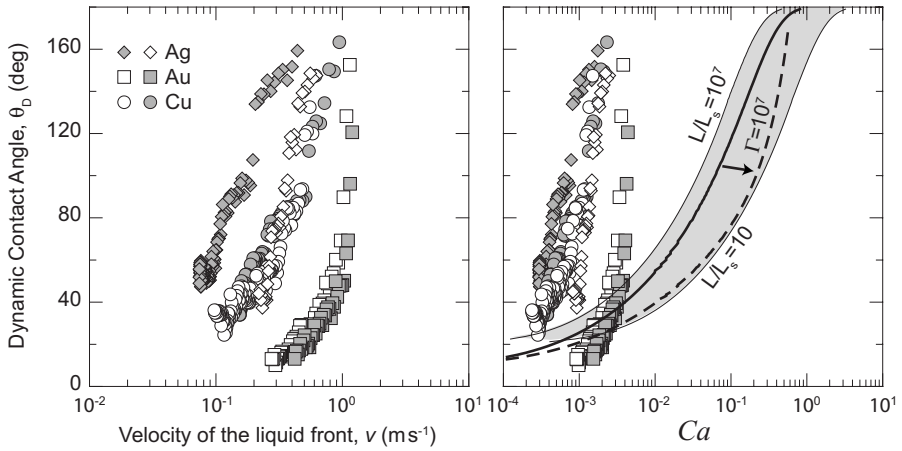

FIG. 12. Velocity and corresponding capillary number recorded for the spreading of liquid metals on Mo. Spreading is much slower than expected for simple hydrodynamic models (shadowed area, $\theta_0=20°$). The continuous line shows the relationship between Ca and θ_D for $L/L_s=10^4$ according to Eqs. (9) and (10). The dashed line shows the modification of this relationship for the same L/L_s values when inertial effects are taken into account, following Cox analysis (for $\Gamma=10^7$) [75].

$$\gamma_{lv}(\cos\theta_0-\cos\theta_D)+\varphi(v)\ll 2nkT, \tag{14}$$

Eq. (13) transforms into

$$v=\frac{\gamma_{lv}}{\zeta}[(\cos\theta_0-\cos\theta_D)+\varphi(v)] \tag{15}$$

with

$$\zeta=\frac{kT}{K_0\lambda^3}=\frac{h}{\lambda^3}e^{(\Delta G_w/NkT)}. \tag{16}$$

When $\varphi(v)\sim 0$, a parallel can be drawn between the viscosity η, which can be viewed as a friction coefficient between interior layers of the liquid, and ζ, which is also defined as a friction coefficient between the liquid and the solid. It can be observed that for most of the spreading process recorded with the drop transfer setup, there is a linear relationship between the contact angle and the speed of the liquid metal front (Fig. 13). In order for this to happen with liquid metals, where $\gamma_{lv}\sim 1$ J m^{-2} and $T\sim 10^3$ K, λ should be of the order of the interatomic distances (1 Å), and the capillary driving force should be dominant $\varphi(v)\ll\cos\theta_0-\cos\theta\ll 2nk_bT$. This linear relationship has been observed for all metals, independent of their density, and for all drop sizes investigated in this work. As $\theta_D\to 180°$, deviations of the linear behavior can be expected due to the increasing value of $\cos\theta_0-\cos\theta$, the increasing importance of the surface curvature in the spreading driving force, and the experimental errors associated with the estimation of the speed as $t\to 0$ and the measurements of very large obtuse angles. Similar spreading kinetics have been found for metals in soluble or even reactive systems [18,77].

The calculated friction coefficients are summarized in Table IV. The corresponding maximum velocities of spreading [the spreading velocity when $\theta_D\sim 180°$, $\sim 2\gamma_{lv}/\zeta$, according to Eq. (15)] are of the order of 0.1–1 m s^{-1}, close to what has been experimentally measured (Fig. 12). It can be observed that the friction coefficients are similar for "clean"

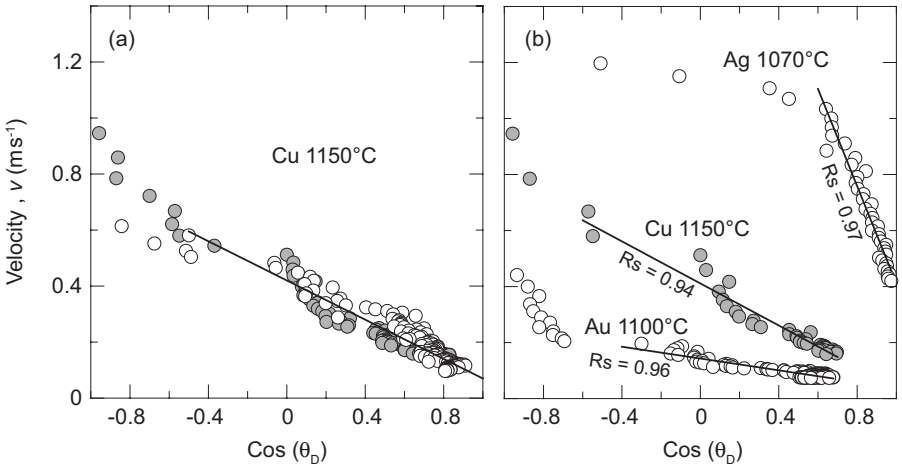

FIG. 13. Spreading kinetics of liquid metals on Mo. (a) Comparison of two experiments for Cu at 1150 °C. (b) Comparison between different metals (residual sum of squares, Rs, for each linear fitting is included). There is a wide range of dynamic contact angles for which there is a linear relationship between θ_D and v.

TABLE IV. Friction coefficients and corresponding atomic frequencies calculated from individual experiments for the nonreactive metal-Mo systems.

Liquid	Substrate	Temperature (°C)	Friction coefficient, ζ (Pa s)	Atomic Frequencies, K_0 (Hz)
Ag	*p*-Mo ("dirty")	960	3.7±0.9	2×10^9
Ag	*p*-Mo ("dirty")	1070	1.5±0.1	5×10^9
Ag	*p*-Mo (clean)	1070	0.8±0.1	8×10^9
Ag	*p*-Mo ("dirty")	1150	1.4±0.1	5×10^9
Ag	*p*-Mo (clean)	1150	0.7±0.2	1×10^{10}
Ag	*p*-Mo (clean)	1290	0.3±0.1	3×10^{10}
Ag	Sc–Mo (110)	960	1.90±0.1	3×10^9
Ag	Sc–Mo (110)	1290	0.5±0.1	2×10^{10}
Au	*p*-Mo (clean)	1100	17.2±0.5	4×10^8
Au	*p*-Mo (clean)	1100	24±1	3×10^8
Cu	*p*-Mo ("dirty")	1100	2.5±0.3	3×10^9
Cu	*p*-Mo (clean)	1150	3.6±0.3	2×10^9
Sn	*p*-Mo	1190	4.2±0.3 [51]	2×10^9
Water and/or glycerol	PET	Room temp	0.01–1.2 [7]	10^7-10^9
Silicone oils	glass	Room temp	35–3600 [7]	10^3-10^5

and "dirty" Mo surfaces. Friction for the different metals is very similar with the exception of gold, which shows a larger value. The frictions are also much larger than reported values for organic liquids of similar viscosities (Table IV). Due to its lower melting point, spreading data with silver have been collected over a wider range of temperatures. There is a strong dependence of the friction coefficient with temperature. In both Eqs. (6) and (7), the dependence of spreading kinetics on temperature is given by $\gamma_{lv}(T)/\rho(T)$. This dependence is not very strong; for silver, the factor changes less than 2% in the range of temperatures used in this study [32,78]. This temperature dependence supports the hypothesis that the physical processes occurring at the triple line are playing a dominant role. For silver, it is possible to use a linear fitting of $\ln(\zeta)$ vs $1/T$ to calculate independently the distance between adsorption sites and the wetting activation energy (Fig. 14). The calculated distances between adsorption sites are $\lambda \approx 1.4\pm0.7$ Å, of the order of the molybdenum atomic radii (1.4 Å) [78], and the wetting activation energies are of the order of $\sim 97\pm16$ kJ mol^{-1}. The calculated value of λ is of the order of interatomic distances. It must be pointed out that small variations in λ will not greatly affect the calculated wetting activation energy. For example, the calculated ΔG_w, by taking $\lambda=3.14$ Å (the interatomic distance in Mo [78]), is ~ 120 kJ mol^{-1}. Fixing $\lambda=1.4$ Å, the resulting wetting activation energies vary between ~ 130 kJ mol^{-1} for gold and ~ 110 kJ mol^{-1} for copper. Analysis of tin data taken from Naidich *et al.* [51] results in similar wetting activation energy: ~ 120 kJ mol^{-1}. The corresponding equilibrium frequencies are 10^8-10^{10} s^{-1}.

2. Spreading of glasses

As expected from their larger viscosities, the spreading of silicate glasses is much slower than the spreading of liquid metals. The behavior observed using the drop transfer setup and the sessile drop configuration is very similar, although in the drop transfer experiments, the initial stages of spreading (very large dynamic contact angles) can be recorded. In all cases, equilibrium contact angles were reached after 4 to 12 min (Fig. 15). There was no indication of the existence of a precursor foot, as it has been reported for other glass and/or metal systems [79], or of the formation of triple-line ridges.

It is clear that glass spreading occurs in the capillary regime (Oh $\sim 10^2-10^3$, Table III), the spreading velocities are much slower, and the drops maintain a constant curvature shape. As for the metals, the spreading velocities of the

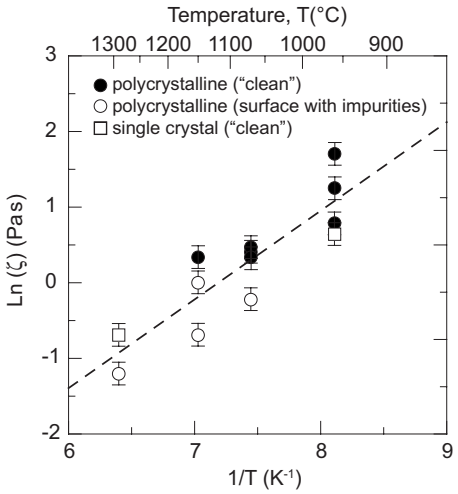

FIG. 14. Dependence of the friction coefficient for silver with temperature. Each point corresponds to a single experiment. The final contact angle has been used to separate clean surfaces from those with remaining adsorbed impurities.

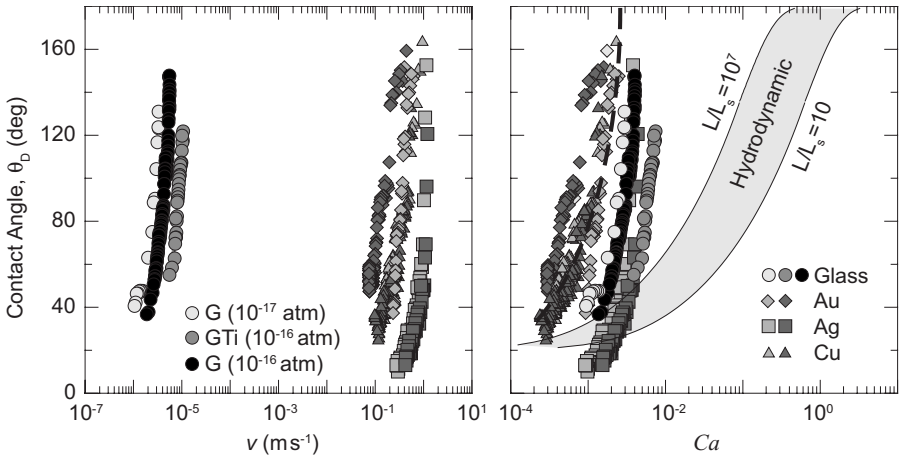

FIG. 15. (a) Spreading velocities of molten oxides (glasses) on Mo at 1200 °C (the oxygen partial pressures during the experiments are indicated in the figure). Metal data are also plotted for comparison. (b) Corresponding capillary numbers. The dashed line corresponds to a curve generated using the molecular kinetic model [Eq. (11)] with $\theta_0=0°$, T=1100 °C, $\lambda\sim 1$ Å, $\gamma_{sl}\sim 1$ J m^{-2} and $K_0\sim 3\times 10^7$ s^{-1}.

glasses are slower than can be expected from simple hydrodynamic models (Fig. 15). By plotting the spreading velocity vs $\cos(\theta_D)$ (Fig. 16), it is possible to calculate a friction coefficient (ζ) of the order of $\sim 10^5$ Pa s, orders of magnitude larger than what has been measured for the liquid metals (Fig. 16). By taking $\lambda\sim 1.5$ Å, then the measured wetting activation energy are 200–300 kJ mol^{-1}, which is of the order of the activation energy for viscous flow in these liquids ($\sim$290–300 kJ mol^{-1}) [27,80].

Because the spreading velocities are slow, inertia is negligible, and the drop surface maintains constant curvature during spreading, it is possible to use the combined model proposed by de Ruijter and co-workers [81–83] to treat simultaneously the viscous and triple-line dissipation. According to their analysis, when both the molecular kinetic theory and the hydrodynamic analyses are taken into account, then

$$v = \frac{\gamma(\cos\theta_0 - \cos\theta_D)}{\zeta + 6\eta\Phi(\theta_D)\ln\left(\frac{R}{a}\right)}, \tag{17}$$

with Φ being a geometrical term that relates the base radius of the drop, R, to its volume,

$$\Phi(\theta) = \frac{\sin^3\theta_D}{2 - 3\cos\theta_D + \cos^3\theta_D}. \tag{18}$$

The quantity a is a cutoff length, below which the viscous dissipation in the core of the drop is considered to be negligible. The time evolution of the contact angle is then given by

$$\frac{d\theta}{dt} = \frac{d\theta}{dr}\frac{dr}{dt} = \left(\frac{\pi}{3V}\right)^{1/3}(\{\Phi(\theta_D)^{1/3}\}')^{-1}\frac{\gamma(\cos\theta_0 - \cos\theta_D)}{\zeta + 6\eta\Phi(\theta_D)\ln\left(\frac{R}{a}\right)}. \tag{19}$$

As done with pure molecular kinetic theory, this model was validated both experimentally and by molecular dynamic simulations.

By fitting the glass data to these equations (Fig. 17), an estimate of the values for ζ and $\ln(R/a)$ can be obtained Again, the triple-line friction coefficient is $\sim 3-7\times 10^5$ Pa s. These values are similar to those calculated when assuming that triple-line friction was the sole source of dissipation, reinforcing the hypothesis that friction is playing a

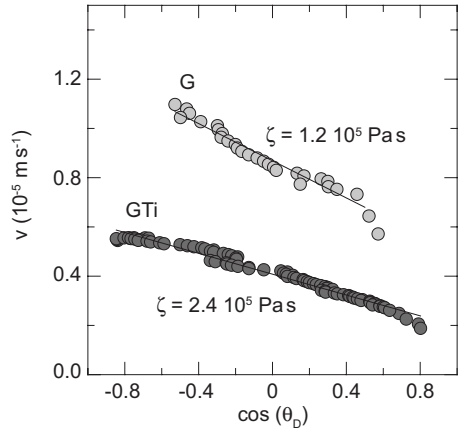

FIG. 16. Velocity of spreading vs dynamic contact angle in two different experiments for silicate glasses on molybdenum.

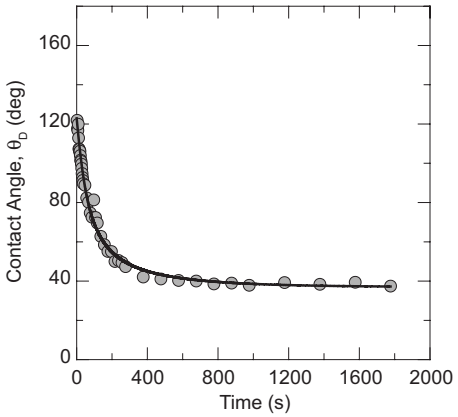

FIG. 17. Fitting of the contact angle of glass (G) on Mo according to Eq. (21). The points are the experimental data.

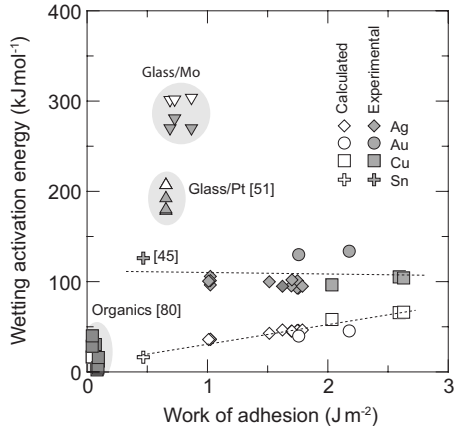

FIG. 18. Calculated (open symbols) and experimental wetting activation energies for metals and glasses on Mo. Each value corresponds to an individual experiment. The calculated values add the contributions from the solid-liquid [Eq. (22)] and the liquid-liquid (activation energies for viscous flow). The calculated values for metals are always lower than the experimental ones. Typical experimental data for organic systems (such as water, silicone oils, etc.) are plotted for comparison.

dominant role. The calculated value of the coefficient R/a, $\sim 10^9$, is consistent with the cutoff length $a \sim 0$.

IV. FINAL CONSIDERATIONS

It is usually assumed in the molecular kinetic analysis of spreading that the wetting activation energy has two contributions: one coming from the solid-liquid interactions (ΔG_w^{sl}), and the other from the liquid-liquid interactions (ΔG_w^{ll}) [26,84]. The contribution from the liquid-liquid interactions is of the order of the activation energy for viscous flow. For liquid metals, this ranges between 16 kJ mol^{-1} for gold and 30 kJ mol^{-1} for Cu, while for the glasses, they are of the order of the activation energy for viscous flow in these materials ($\sim$290–300 kJ mol^{-1}).

For metals, the activation energy for viscous flow is much lower than the measured ΔG_w, indicating that solid-liquid interactions have a dominant contribution to the wetting activation energy. Blake and de Coninck [84] used the work of adhesion to estimate the strength of the solid-liquid interactions, and their contribution to the free wetting activation energy. According to their analysis

$$\Delta G_w \approx N\lambda^2 W_{ad}. \tag{20}$$

In the metallic systems, $W_{ad} \sim 1$–3 J m^{-2}, meaning that if $\lambda \sim 1$ Å, then $\Delta G_w^{sl} \sim 10$ kJ mol^{-1} [taking a larger λ, in the range of nanometers or more, will result in very large wetting activation energies (Fig. 18), reinforcing the idea that the critical step size for the spreading process is of the order of interatomic distances]. The calculated wetting activation energies are lower than measured experimentally. With the exception of gold, which exhibits a significantly larger friction, the experimental values are similar for the different metals. It is possible that, due to adsorption, the work of adhesion is not the best magnitude to compare the strength of the solid-liquid interactions (ε_{sl}). Following a reasoning similar to the one described by Blake and de Coninck [84], it could be expected that $\Delta G_w \alpha \varepsilon_{\mathrm{Mo}Me}$. If Ω is the regular solution parameter,

$$\Omega = zN\left(\varepsilon_{\mathrm{Mo}Me} - \frac{1}{2}(\varepsilon_{MeMe} + \varepsilon_{\mathrm{MoMo}})\right), \tag{21}$$

where $\varepsilon_{\mathrm{MoMo}}$ and ε_{MeMe} are the bonding energies of the metal and Mo, respectively, then for a series of liquids on Mo, the wetting activation energy will be approximately proportional to $\Omega - (L_s^{\mathrm{Mo}} + L_s^{Me})$. According to Tables III and IV, the friction of the different metals roughly follows the expected trend. The solution parameter is much smaller in the Au-Mo case, indicating much stronger solid-liquid interactions and resulting in larger frictions. Nevertheless, copper and silver have different solution parameters, but the frictions are similar. It is clear that in order to fully model the process, it will be necessary to define the critical atomic step that controls spreading kinetics. Blake, for example, proposed that the triple junction moves through an adsorption-desorption mechanism [26]; however, measured desorption activation energies in these systems (300–400 kJ mol^{-1}) are significantly larger than the solid-liquid contribution to the wetting activation energy that seems to be closer to the value of activation energies for surface diffusion in metal-metal systems ($\sim$100 kJ mol^{-1}) [85–89].

For glasses, the calculated wetting activation energies are of the order of the activation energies for viscous flow. This suggests that during the spreading of molten oxides, the liquid-liquid interactions play a double role: on one hand, they have a significant (probably dominant) contribution to the triple-line friction; on the other, they control the viscous dissipation in the bulk drop.

The combined models for spreading have the great advantage of presenting a clear understanding of the relative importance of the different dissipation channels. While the dominant channel of dissipation also depends on the dynamic contact angle [Eq. (17)], if $\zeta \gg \eta$, the friction between the solid and the liquid is predominant during most of the spreading, whereas if $\zeta \ll \eta$, viscosity is the leading channel of dissipation. High- and low-temperature systems present some fundamental differences and similarities. The range of liquid viscosities is very similar (Fig. 19); however, the solid-liquid and liquid-liquid interactions are much stronger at high temperature, resulting in works of adhesion and surface tensions that are typically two orders of magnitude larger than for organic liquids with similar viscosity. As a result, the triple-line friction of liquids of similar viscosity is much larger at high temperature; for example, typical friction values reported for water on diverse substrates are of the order of 10^{-2} Pa s, whereas for liquid metals with similar viscosity, they are 1–10 Pa s. Still, Roux and Cooper-White [90] have already indicated that even for waterdrops deposited on glass, solid-liquid interactions can play a role in the dissipation of the initial kinetic energy.

Simple models relating the work of adhesion to the contribution of the solid-liquid interactions to the triple-line friction result in values that are of the order of those measured

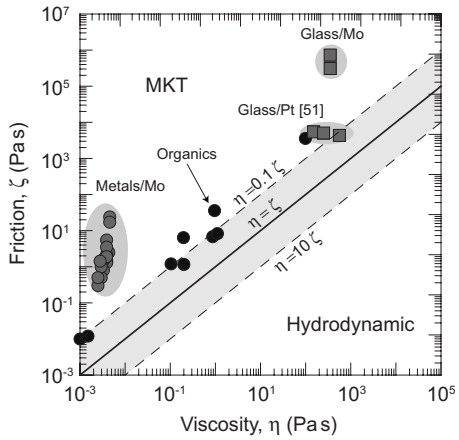

FIG. 19. Friction vs viscosity for high- and some low-temperature (black circles) systems. Data for glasses on Mo has been calculated using the combined model. For the metals and glasses on Mo, the friction is at least two orders of magnitude larger than the viscosity. This is consistent with a scenario in which spreading is controlled by the atomic dynamics at the triple junction. For some organic liquids (and for the glass on Pt studied by Hockings [55]) friction and viscosities are closer. The dominant dissipation channel depends on the characteristics of the systems, and the dynamic contact angle e.g., term $6\eta\Phi(\theta_D)\ln(R/a)$ in Eq. (17), and combined models are needed to provide a complete description of spreading.

experimentally; however, for metals, the theoretical values are slightly lower than experimentally measured. It could be that, due to the adsorption effects, the work of adhesion (or the work of separation that we are measuring in our experiments) provides only a first approximation to the strength of solid-liquid interactions. In addition, it is necessary to define the critical atomic step that controls the movement of the triple junction. It is interesting to observe that the theoretical and experimental values seem to converge as the melting point of the metal increases; this could be due to the fact that as the temperature increases, so does the work of adhesion and its role on the triple-line friction, or to the decreasing importance of adsorption.

V. SUMMARY

This analysis of nonreactive spreading of molten metals and glasses on Mo illustrates the fundamental similarities and differences between the movement of a liquid front at high and low temperature, and establishes that the strength of atomic interactions determines the dominant dissipation channels that control spreading kinetics. Stronger interatomic forces in high-temperature systems result in an increased role of triple-line friction vs viscous dissipation in bulk liquid. Solid-liquid and liquid-liquid interactions both contribute to triple-line friction. Liquid metals have lower viscosities, and the interactions between the liquid and the substrate are the main contribution to friction, whereas for highly viscous molten oxides, interactions between the liquid molecules play a dominant role. In the latter case, viscosity affects spreading in two ways: through the viscous impedance in the liquid, and through its contribution to the triple-line friction. These results can serve as the basis for the formulation of a unified theory of spreading in high- and low-temperature systems, and as a first step in the analysis of more complex, reactive systems, such as those of interest in many technological applications, from brazing to soldering or composite fabrication.

ACKNOWLEDGMENTS

This work was supported by the Director, Office of Science, Office of Basic Energy Sciences, Materials Sciences and Engineering Division, of the U.S. Department of Energy under Contract No. DE-AC02-05CH11231. S. L.-E. has been supported by the Spanish Ministry of Education and Science under the Ramon y Cajal Program. We gratefully thank Dr. Wilfried Sigle and Rowland Cannon for their fruitful discussions.

[1] P. G. de Gennes, Rev. Mod. Phys. **57**, 827 (1985).
[2] F. Brochard-Wyard, D. Quere, and P.-G. d. Gennes, *Capillarity and Wetting Phenomena: Drops, Bubbles, Pearls, Waves* (Springer, New York, 2004).
[3] J. C. Berg, *Wettability* (Dekker, New York, 1993).
[4] N. Eustathopoulos, M. G. Nicholas, and B. Drevet, *Wettability at High Temperatures* (Pergamon, Amsterdam, 1999).
[5] F. M. Fowkes and W. Zisman, *Symposium on Contact angle, wettability, and adhesion*, Los Angeles, California, 1963 (American Chemical Society, Washington, 1964).
[6] F. G. Yost, F. M. Hosking, and D. R. Frear, *The Mechanics of Solder Alloy Wetting and Spreading* (Van Nostrand Reinhold, New York, 1993).
[7] T. D. Blake, J. Colloid Interface Sci. **299**, 1 (2006).
[8] N. Eustathopoulos, Curr. Opin. Solid State Mater. Sci. **9**, 152 (2005).
[9] E. Saiz, R. M. Cannon, and A. P. Tomsia, Acta Mater. **48**, 4449 (2000).
[10] I. A. Aksay, C. E. Hoge, and J. A. Pask, J. Phys. Chem. **78**, 1178 (1974).
[11] Y. Naidich, Curr. Opin. Solid State Mater. Sci. **9**, 161 (2005).
[12] J. C. Ambrose, M. G. Nicholas, and A. M. Stoneham, Acta Metall. Mater. **40**, 2483 (1992).
[13] F. G. Yost, Scr. Mater. **38**, 1225 (1998).
[14] W. J. Boettinger, C. A. Handwerker, and U. R. Kattner, in *The Mechanics of Solder Alloy Wetting and Spreading*, edited by F. G. Yost, F. M. Hosking, and D. R. Frear (Kluwer Academic Publishers, Boston, 1993), p. 103.
[15] N. Sobczak, M. Singh, and R. Asthana, Curr. Opin. Solid State Mater. Sci. **9**, 241 (2005).
[16] R. E. Loehman *et al.*, J. Mater. Sci. **40**, 2319 (2005).
[17] J. A. Warren, W. J. Boettinger, and A. R. Roosen, Acta Mater. **46**, 3247 (1998).
[18] E. Saiz and A. P. Tomsia, Nat. Mater. **3**, 903 (2004).

[19] L. Yin, S. J. Meschter, and T. J. Singler, Acta Mater. **52**, 2873 (2004).
[20] L. Yin, B. T. Murray, and T. J. Singler, Acta Mater. **54**, 3561 (2006).
[21] E. B. I. Webb *et al.*, Acta Mater. **53**, 3163 (2005).
[22] E. B. Webb, J. J. Hoyt, and G. S. Grest, Curr. Opin. Solid State Mater. Sci. **9**, 174 (2005).
[23] E. B. Webb, G. S. Grest, and D. R. Heine, Phys. Rev. Lett. **91**, 236102 (2003).
[24] N. Eustathopoulos, Acta Mater. **46**, 2319 (1998).
[25] S. F. Kistler, in *Wettability*, edited by J. C. Berg (Dekker, New York, 1993), p. 311.
[26] T. D. Blake, in *Wettability* [25], p. 251.
[27] S. Lopez-Esteban *et al.*, Langmuir **21**, 2438 (2005).
[28] L. Gremillard *et al.*, J. Mater. Res. **21**, 3222 (2006).
[29] Outokumpu Research, Pori, Finland, 1993.
[30] E. Saiz, A. P. Tomsia, and R. M. Cannon, Acta Mater. **46**, 2349 (1998).
[31] E. Saiz, A. P. Tomsia, and R. M. Cannon, Scr. Mater. **44**, 159 (2001).
[32] B. J. Keene, Int. Mater. Rev. **38**, 157 (1993).
[33] T. Sugita, S. Ebisawa, and K. Kawasaki, Surf. Sci. **20**, 417 (1970).
[34] Y. Naidich, in *Progress in Surface and Membrane Science*, edited by D. A. Candenhead and J. F. Danielli (Academic Press, New York, 1981), Vol. 14, p. 353.
[35] M. Nicholas and D. M. Poole, J. Mater. Sci. **2**, 269 (1967).
[36] B. C. Allen, J. Less-Common Met. **29**, 263 (1972).
[37] A. P. Tomsia, E. Saiz, B. J. Dalgliesh, and R. M. Cannon, in 4th Japan International SAMPE Symposium (Society for the Advancement of Material and Process Engineering, Tokyo, Japan 1995), p. 347.
[38] N. Rauch, E. Saiz, and A. P. Tomsia, Z. Metallkd. **94**, 233 (2003).
[39] J. G. Che, C. T. Chan, W. E. Jian, and T. C. Leyns, Phys. Rev. B **57**, 1875 (1998).
[40] M. Methfessel, D. Hennig, and M. Scheffler, Phys. Rev. B **46**, 4816 (1992).
[41] A. Skapski, Acta Metall. **4**, 576 (1956).
[42] Y. V. Naidich, N. F. Grigorenko, and V. M. Perevertailo, J. Cryst. Growth **53**, 261 (1981).
[43] G. Levi, C. Scheu, and W. D. Kaplan, Interface Sci. **9**, 213 (2001).
[44] P. Wynblatt, Acta Mater. **48**, 4439 (2000).
[45] C. Serre *et al.*, Metall. Mater. Trans. A **32**, 2851 (2001).
[46] E. Ricci and A. Passerone, Mater. Sci. Eng., A **161**, 31 (1993).
[47] L. Coudurier *et al.*, Acta Metall. **26**, 465 (1978).
[48] E. Saiz, A. P. Tomsia, and R. M. Cannon, in *Ceramic Microstructures. Control at the Atomic Level*, edited by A. P. Tomsia and A. M. Glaeser (Plenum Press, New York, 1998), p. 65.
[49] D. Chatain *et al.*, J. Am. Ceram. Soc. **76**, 1568 (1993).
[50] D. Chatain *et al.*, J. Am. Ceram. Soc. **77**, 197 (1994).
[51] Y. V. Naidich, W. Sabuga, and V. M. Perevertailo, Adgeziya Raspl. Pajka. Mater. **27**, 23 (1992).
[52] J. G. Li, J. Am. Ceram. Soc. **75**, 3118 (1992).
[53] V. K. Nagesh, A. P. Tomsia, and J. A. Pask, J. Mater. Sci. **18**, 2173 (1983).
[54] J. E. Lazaroff, P. D. Ownby, and D. A. Weirauch, Jr., J. Am. Ceram. Soc. **78**, 539 (1995).
[55] L. M. Hocking and A. D. Rivers, J. Fluid Mech. **121**, 425 (1982).
[56] L. Gremillard *et al.*, Z. Metallkd. **95**, 261 (2004).
[57] F. Gentner *et al.*, Langmuir **20**, 4748 (2004).
[58] A. L. Biance, C. Clanet, and D. Quere, Phys. Rev. E **69**, 016301 (2004).
[59] B. Lavi and A. Marmur, Colloids Surf., A **250**, 409 (2004).
[60] M. D. Lelah and A. Marmur, J. Colloid Interface Sci. **82**, 518 (1981).
[61] S. Schiaffino and A. A. Sonin, Phys. Fluids **9**, 3172 (1997).
[62] R. Rioboo *et al.*, J. Mater. Sci. **41**, 5068 (2006).
[63] L. Duchemin, J. Eggers, and C. Josserand, J. Fluid Mech. **487**, 167 (2003).
[64] J. Eggers, J. R. Lister, and H. A. Stone, J. Fluid Mech. **401**, 293 (1999).
[65] D. G. A. L. Aarts *et al.*, Phys. Rev. Lett. **95**, 164503 (2005).
[66] R. G. Cox, J. Fluid Mech. **168**, 169 (1986).
[67] O. V. Voinov, Izv. Akad. Nauk SSSR, Mekh. Zhidk. Gaza **5**, 76 (1976).
[68] T. D. Blake and J. M. Haynes, J. Colloid Interface Sci. **29**, 174 (1969).
[69] M. J. de Ruijter *et al.*, Langmuir **13**, 7293 (1997).
[70] J. De Coninck, M. J. de Ruijter, and M. Voue, Curr. Opin. Colloid Interface Sci. **6**, 49 (2001).
[71] B. Efron and G. Gong, Am. Stat. **37**, 36 (1983).
[72] A. Savitzky and M. J. E. Golay, Anal. Chem. **36**, 1627 (1964).
[73] M. Benhassine, D. Seveno, and J. De Coninck (private communication).
[74] E. B. Dussan and S. H. Davis, J. Fluid Mech. **65**, 71 (1974).
[75] R. G. Cox, J. Fluid Mech. **357**, 249 (1998).
[76] T. D. Blake *et al.*, Colloids Surf., A **149**, 123 (1999).
[77] E. Saiz *et al.*, Acta Mater. **51**, 3185 (2003).
[78] C. J. Smithells and E. A. Brandes, *Metals Reference Book* (Butterworths, London, 1976).
[79] W. Radigan *et al.*, J. Colloid Interface Sci. **49**, 241 (1974).
[80] Y. Kawai and Y. Shiraishi, *Handbook of Physico-chemical Properties at High Temperatures* (The Iron and Steel Institute of Japan, Tokyo, 1988).
[81] M. J. de Ruijter, T. D. Blake, and J. De Coninck, Langmuir **15**, 7836 (1999).
[82] M. J. de Ruijter *et al.*, Langmuir **16**, 2363 (2000).
[83] M. J. de Ruijter, J. De Coninck, and G. Oshanin, Langmuir **15**, 2209 (1999).
[84] T. D. Blake and J. De Coninck, Adv. Colloid Interface Sci. **96**, 21 (2002).
[85] E. G. Seebauer and C. E. Allen, Prog. Surf. Sci. **49**, 265 (1995).
[86] S. H. Payne *et al.*, Surf. Sci. **345**, L1 (1996).
[87] E. V. Goeler and E. Luscher, J. Phys. Chem. Solids **24**, 1217 (1963).
[88] M. Paunov and E. Bauer, Appl. Phys. A: Solids Surf. **44**, 201 (1987).
[89] A. Pavlovska, H. Steffen, and E. Bauer, Surf. Sci. **195**, 207 (1988).
[90] D. C. D. Roux and J. J. Cooper-White, J. Colloid Interface Sci. **277**, 424 (2004).
[91] A. K. Niessen, F. R. de Boer, R. Boom, P. F. de Chatel, W. C. M. Mattens, and A. Miedema, CALPHAD: Comput. Coupling Phase Diagrams Thermochem. **7**, 51 (1983).